SCIENTIFIC REPORTS

OPEN

Studying hydrogen bonding and dynamics of the acetylate groups of the Special Pair of *Rhodobacter sphaeroides* WT

Daniel Gräsing[1], Katarzyna M. Dziubińska-Kühn[1], Stefan Zahn[2], A. Alia[3,4] & Jörg Matysik [1]

Although the cofactors in the bacterial reaction centre of *Rhodobacter sphaeroides* wild type (WT) are arranged almost symmetrically in two branches, the light-induced electron transfer occurs selectively in one branch. As origin of this functional symmetry break, a hydrogen bond between the acetyl group of P_L in the primary donor and His-L168 has been discussed. In this study, we investigate the existence and rigidity of this hydrogen bond with solid-state photo-CIDNP MAS NMR methods offering information on the local electronic structure due to highly sensitive and selective NMR experiments. On the time scale of the experiment, the hydrogen bond between P_L and His-L168 appears to be stable and not to be affected by illumination confirming a structural asymmetry within the Special Pair.

The reaction centre (RC) of the purple bacterium *Rhodobacter (R.) sphaeroides* is a membrane protein in which the primary charge separation, the first step of photosynthesis, is taking place. The availability of the x-ray structure of the RCs of this purple bacterium was a major break-through for the understanding of the early processes in photosynthesis[1]. The cofactors associated with the M- and L-subunits of bacterial RCs are arranged in two nearly symmetric branches spanning the membrane. Each branch consists of two bacteriochlorophylls *a*, a bacteriopheophytin *a* and a quinone. At the end of the branches, a non-heme iron is located (Fig. 1). Close to the B-branch and bound to the M subunit, a carotenoid molecule is present breaking the symmetry of the two branches.

The primary electron-donor P, the so-called Special Pair, is formed by two overlapping bacteriochlorophylls *a*, P_L and P_M. Upon illumination, the Special Pair becomes electronically excited and transfers an electron to the ubiquinone Q_A via an accessory bacteriochlorophyll *a* (B_A) and a bacteriopheophytin *a* (Φ_A). In the final step, the electron is transferred to Q_B. Two photocycles coupled with the uptake of two protons reduce Q_B to Q_BH_2 which diffuses out of the protein into the membrane-based quinone pool.

Although the two branches A and B are nearly symmetric, the electron transfer occurs selectively via the A-branch[2,3]. The directional electron transfer is reflected in the asymmetry of the electronic structure of the Special Pair in the various electronic states. In cation radical state $P^{\bullet+}$ reflecting the HOMO, techniques as EPR, ENDOR and solid-state photo-CIDNP NMR show more unpaired electron spin density on P_L than on P_M[4–7]. The localization of the LUMO mainly on cofactor P_M, from which the electron transfer occurs, has been explored by the photo-CIDNP MAS NMR analysis of the donor triplet state ^3P[8]. This asymmetry is already present in the electronic ground-state of the supermolecule P, as demonstrated by differences in chemical shifts[9–13].

Mutagenesis as well as theoretical studies established that the orientation and coordination C-3^1-acetyl groups of P_L and P_M affect the electronic structure and the redox potential of the special pair[14–16]. As there is no hydrogen bonding partner available, the x-ray structures and Raman spectroscopy data of the acetyl group of P_M also show no involvement in any coordination as the Mg-O distance is about 3.3 ± 0.3 Å, while this distance shrinks to 2.4 Å in QM/MM studies "*essentially forming a sixth ligand to the metal*"[17–20]. On the other hand, Raman spectroscopic and QM/MM studies on specifically mutated RC showed that the orientation of the acetyl group of P_L depends on the protonation state of His-L168 as it is either involved in a hydrogen bond to His-L168 or, if no hydrogen

[1]Institut für Analytische Chemie, Universität Leipzig, Linnéstraße 3, D-04103, Leipzig, Germany. [2]Leibniz Institute of Surface Engineering (IOM), Permoserstraße 15, D-04318, Leipzig, Germany. [3]Institut für Medizinische Physik und Biophysik, Universität Leipzig, Härtelstr. 16-18, D-04107, Leipzig, Germany. [4]Leiden Institute of Chemistry, Leiden University, Einsteinweg 55, 2301 RA, Leiden, The Netherlands. Correspondence and requests for materials should be addressed to J.M. (email: joerg.matysik@uni-leipzig.de)
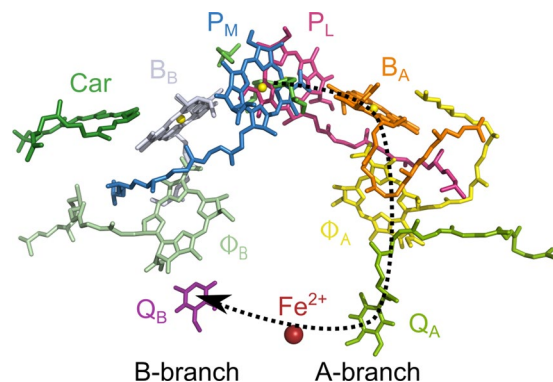
Figure 1. Cofactor arrangement in the RC of *R. sphaeroides* WT: P_M and P_L — bacteriochlorophyll *a* dimer, forming the primary electron donor, the Special Pair P, $B_{A/B}$ — accessory bacteriochlorophyll *a*, $\Phi_{A/B}$ — bacteriopheophytin *a*, $Q_{A/B}$ — quinone A and terminal electron accepting quinone B, Fe^{2+} — non-heme iron, Car — carotenoid. The electron is transferred only via the A-branch (black arrow). For details, see text.
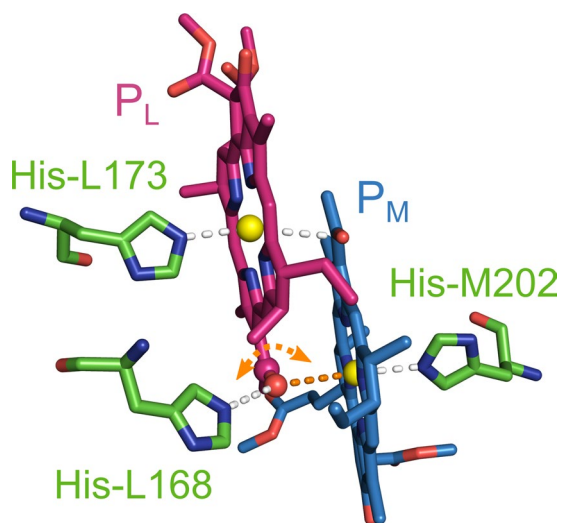

Figure 2. View on the Special Pair with the coordinating histidines. Depending on the protonation state of His-L168, the acetyl group of P_L can either be involved in a hydrogen bond (white) or coordinating the magnesium ion of P_M (orange). The coordination of the acetyl group might change upon electron transfer (orange arrow), tuning the electronic properties of the Special Pair during its photocycle. The acetyl group of P_M is always coordinated to the magnesium ion of P_L since no other coordination partner is available.

bond is available, located very close to the magnesium ion of P_M (Fig. 2)[18,21–23]. It was therefore suggested that a re-orientation of the acetyl group of P_L acts as a valve to block the electron back-transfer upon cleavage of the hydrogen bond to His-L168 and thereby re-tuning of the electronic properties of the Special Pair[16]. The acetyl group might therefore be involved in the reorientation of protein polar groups that lead to electric polarization effects during the radical-pair formation[24–26]. So far, no experimental evidence on the cleavage or the dynamics of the hydrogen bond is known, since no appropriate method with enough sensitivity was available.

Nuclear magnetic resonance (NMR) spectroscopy can be a major technique to probe local dynamics. The lack of sensitivity usually related to this method, can be overcome by the solid-state photo-CIDNP effect allowing to study the photosynthetic cofactors in their native environment[27,28]. The solid-state photo-CIDNP effect induces a non-Boltzmann nuclear spin distribution after a photo-cycle in all natural photosynthetic RC as well as in some flavin proteins[8,29–36]. The enhancement is sufficiently strong to observe particular carbon positions on the cofactors forming the spin-correlated radical pair (SCRP), which is constituted by the donor and the acceptor cofactors, even in entire plants without any further isolation[37]. During the lifetime of the SCRP, multiple coherent mixing mechanisms take place leading to observable nuclear hyperpolarisation in the electronic ground state on the donor and the acceptor molecules. These mechanisms can be explained by level anti-crossings and are termed three-spin mixing (TSM) and differential decay (DD)[38–42]. In case of the quinone-blocked RC of *R. sphaeroides* WT, the Special Pair acts as the donor and the Φ_A is the acceptor (Fig. 3).

In this study, we apply photo-CIDNP MAS NMR experiments to investigate the hydrogen-bond interaction between the acetyl group of P_L and His-L168 by measuring the chemical shift anisotropy (CSA) of C-3^1 of the
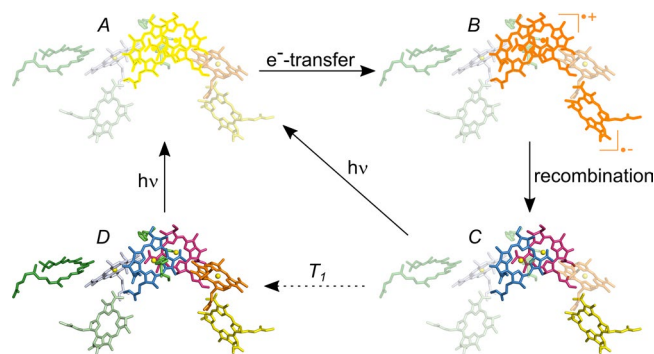
Figure 3. Generation of nuclear hyperpolarisation via the solid-state photo-CIDNP mechanism on the primary donor, the Special Pair P (red and blue), as well as on the primary acceptor Φ_A (yellow) in quinone depleted bacterial RC. The phytyl chains are omitted for sake of clarity. After light excitation of P (**A**), an electron is transferred to the Φ_A forming a spin correlated radical pair (SCRP) (**B**). In this state, nuclear hyperpolarisation is generated which can be observed in the electronic ground-state after recombination (**C**) (for details, see main text). Hyperpolarisation of P and Φ_A is accumulated by a series of photocycles and decays by nuclear T_1 relaxation (**A/D**).

acetyl group and comparing it to DFT calculations to test whether the assumed cleavage of the hydrogen bond between P_L and His-L168 can be experimentally verified.

Methods

Sample preparation.   Cultures of *Rb. sphaeroides* WT were grown anaerobically in the presence of 1.0 mM [3-^{13}C]-δ-aminolevulinic acid • HCl (3-ALA) (Buchem B.V., Apeldoorn, The Netherlands) for selective ^{13}C isotope labelling of BChl a and BPhe as described before [9]. The RCs were isolated and the quinones were removed as described earlier [12]. Approximately 10 mg of RC protein complex embedded in LDAO micelles was used for the NMR experiment.

Solid-state photo-CIDNP MAS NMR.   All NMR experiments have been performed with a double-resonance MAS probe at a Bruker AVANCE III spectrometer (Bruker-Biospin, Karlsruhe, Germany) operating at a proton Larmor frequency of 400.15 MHz. The probe was equipped with a light fiber to illuminate the sample during the measurement as described in ref.[27]. As illumination source, a 488-nm continuous-wave laser (Genesis MX488–1000 STM OPS-Laser-Diode System, Coherent Europe B.V., The Netherlands) operating at 1 W was used. The sample was packed in a clear 4-mm sapphire rotor and frozen in the dark at a slow spinning frequency of 800 Hz to ensure a homogenous sample distribution[43].

If not stated differently, NMR experiments were performed at a spinning frequency of 8 kHz with a recycle delay of 4 s and a temperature of 247 K. The $\pi/2$ ^{13}C pulses were applied at radio-frequency (rf) field strength of 72 kHz, while the rf field strength of the heteronuclear SW$_f$-TPPM decoupling was set to 100 kHz[44]. For the 1D experiment, 1024 scans were recorded with an acquisition time of 20 ms. The spectral width was set to 30 kHz, with the offset placed in the centre of the spectrum, if not stated otherwise. For the 2D INADEQUATE experiments, the SR26 sequence with an rf field strength of 52 kHz was applied[45]. One full SR26 cycle was used for DQ excitation and reconversion each, resulting in a total mixing time of 4 ms. To ensure a large spectral width of 46 kHz, STiC phase shifts were used[46]. The carrier was placed at 100 ppm. A total of 640 scans were averaged per each of the 100 t_1 increments collected. The t_2 acquisition time was set to 20 ms. Heteronuclear SW$_f$-TPPM decoupling was used during the t_1 and t_2 acquisition[44]. The SUPER experiment was performed at a spinning frequency of 6 kHz leading to a rf field of 72.72 kHz for CSA recoupling. 192 scans were averaged during each of the four γ-integral points used, leading to a total number of scans of 768. A total of 32 t_1-increments were recorded. The spectral width was set to 32258.1 Hz taking into account the scaling factor of 0.155[47]. The carrier was placed at 192 ppm. The z-filter for the γ-integral was set to 100 μs. Heteronuclear SW$_f$-TPPM decoupling was used during the t_1 and t_2 acquisition[44]. Frequency discrimination in all 2D experiments was achieved using the States-TPPI method[48].

The simulation of the CSA line shapes were carried out with SIMPSON[49]. The script can be found in the supplementary information.

DFT calculations.   Geometry optimization calculations were based on the crystal structure of Camara-Artigas *et al.* (PDB: 1M3X) and were carried out with the program ORCA 4.0.1.2[50,51]. The resolution of identity approximation in combination with the corresponding auxiliary basis set was employed to speed up the calculation based on the BLYP functional in combination with a def2-SVP basis set[52–54]. The empirical dispersion correction of Grimme 3rd version (with Becke/Johnson) was employed to consider dispersion interactions[55,56]. The protein environment was considered by the conductor-like polarisable continuum model (CPCM) for which a dielectric constant of $\varepsilon = 4$ was selected[57]. The two investigated structural models are shown in the Supplementary Figs S1 and S2. Both models differ in the protonation pattern at His-L168 where solely model A forms a hydrogen bond between His-L168 and P_L, see Fig. S1. The chemical shifts were calculated with the BLYP functional in ADF 2017 using good numerical quality and no frozen core. The empirical dispersion correction
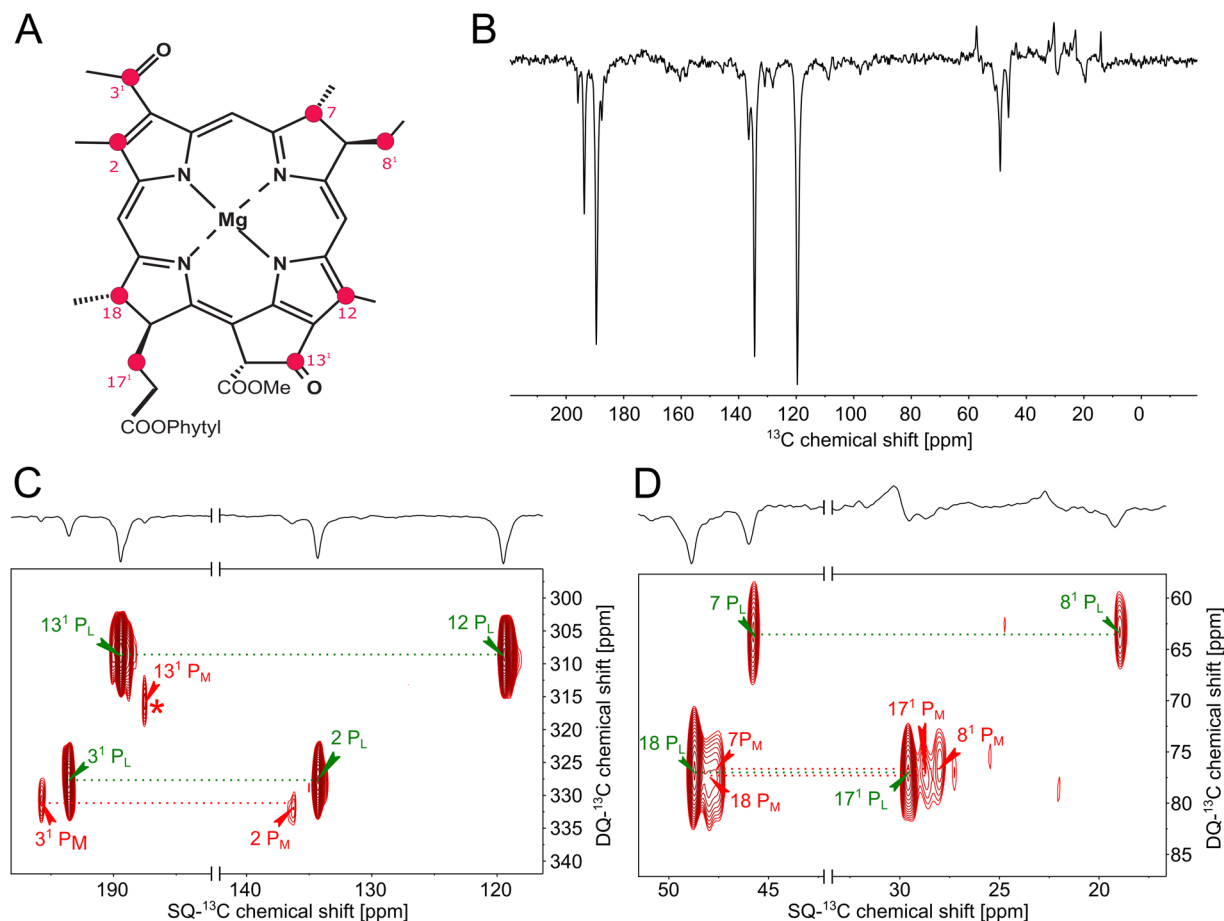
Figure 4. (**A**) Labelling pattern in bacteriochlorophyll *a* achieved by feeding 3-δ-aminolevulinic acid (3-ALA). The atom numeration is according to IUPAC. (**B**) 1D ^{13}C spectra of 3-ALA labeled RC of *R. sphaeroides* WT. (**C,D**) Detailed views on the low (C) and high (D) field regions of the INADEQUATE spectrum of 3-ALA labeled RC of *R. sphaeroides* WT. The double-quantum peak of C-12 P_M correlated to C-13^1 of P_M (marked with an asterisk) was in the range of noise.

of Grimme 3rd version (with Becke/Johnson) was employed to consider dispersion interactions. For protons a single-zeta basis set without polarization was applied. For the carbon atoms a double-zeta singly polarized Slater-type basis set (DZP) was used. Application of a triple-zeta singly polarized Slater-type basis set (TZP) lowered the obtained agreement in isotropic chemical shifts.

Results and Discussion

So far, the assignment of the resonances of the cofactor signals has been performed by comparison of the resonances with the relevant chlorophyll in solution state or by homonuclear DARR or RFDR experiments[9,10,12,58–61]. Comparison to model molecules can lead to wrong assignments due to the drastic effect of the protein matrix on the electronic structure of the Special Pair. Two-dimensional homonuclear experiments on samples with several tetrapyrrole macrocycles might struggle from signal overlap. We therefore apply INADEQUATE experiments to unambiguously assign the resonances as it has already been performed on the 5-ALA labelling pattern[62]. Since the distances are significantly larger in the 3-ALA labelling pattern (Fig. 4A), we used the SR26 sequences which recouples weak dipolar interactions efficiently[45].

Figure 4B shows the 1D spectrum as well as a detailed view on the 2D INADEQUATE spectrum (Fig. 4C,D). As can be seen, a clear correlation between neighbouring labeled carbons up to two bonds apart can be established. This connectivity, the fact that P_L carries more electron density leading to more shielding, as well as the already known assignments from the DARR spectra allow to assign all resonances unambiguously as shown in Table 1. In course of this, due to the observed correlation signal with C-7 of P_L at 64 ppm, we assign the resonance at 19 ppm to C-8^1 of P_L which has been erroneously denoted as C-7^1 in ref.[12]. We do not observe the resonances of C-8^1 of P_L at 32.1 ppm, C-12 of P_M at 128.8 ppm and C-18 of P_M at 50.9 ppm as it was reported earlier[12]. This might be due to the strong field dependence of the solid-state photo CIDNP effect and the different magnetic fields used for both experiments[63,64]. Nevertheless, the SR26 sequence shows a good performance and allows for recoupling over about 2.6 Å (i.e., two bonds) making it suitable for even sparsely labeled samples as they are used in photo-CIDNP MAS NMR.

Position	P_L	P_M
2	134.9 ppm	136.9 ppm
3^1	194.1 ppm	196.3 ppm
7	46.5 ppm	—
8^1	19.7 ppm	28.9 ppm
12	120.0 ppm	—
13^1	188.0 ppm	190 ppm
17^1	30.1 ppm	29.2 ppm
18	49.39 ppm	—

Table 1. Experimentally determined isotropic ^{13}C chemical shifts of the Special Pair in the 3-ALA ^{13}C labeled bacterial RCs of *R. sphaeroides* WT.
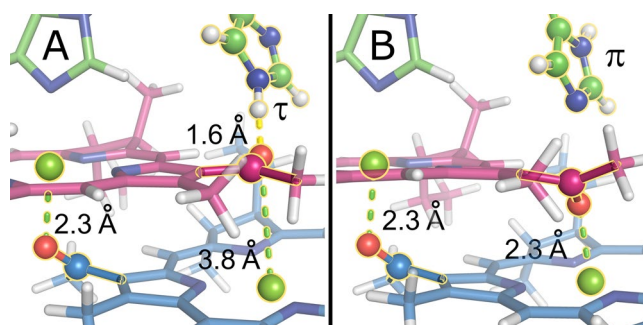

Figure 5. Detailed view on the acetyl group of P_M (blue) and P_L (pink) in the two DFT models. On the left-hand side (model **A**), His-L168 is protonated in the τ-position forming a hydrogen bond of 1.6 Å to the acetyl group of P_L suggesting a moderate hydrogen bonding interaction. The acetyl group of P_M does not have a hydrogen bonding partner and is therefore coordinated to the magnesium ion of P_L. On the right-hand side (model **B**), His-L168 is protonated in the π-position. Lacking a partner for hydrogen bonding, the acetyl group of P_L coordinates to the magnesium ion of P_M. The acetyl group of P_M is always coordinated to the magnesium ion of P_L. The extended presentations of the two models are shown in the Supplementary Information (Supplementary Figs S1 and S2).

Hence, the two C-3^1-acetyl carbons of P_M and P_L have different isotropic chemical shifts, occurring at 194.5 (P_L) and 196.3 ppm (P_M), pointing towards a different chemical environment as, for example, that the acetyl group of P_L has hydrogen bond interaction with His-L168, while the acetyl group of P_M coordinates the magnesium of P_L. To obtain further insight into the chemical environment, we investigated two different DFT models in which His-L168 is protonated at either the τ or the π position (Fig. 5). Depending on the protonation state of His-L168, the acetyl group of P_L is either involved in a hydrogen bond to His-L168 (model A) or it coordinates to the magnesium ion of P_M (model B).

To verify the existence of the hydrogen bond and to explore possible dynamics, we measured the chemical shift anisotropy (CSA) pattern of both groups via the SUPER technique[47]. In highly enriched samples, SUPER reintroduces homonuclear dipolar interactions which in conjunction with J-coupling leads to broadening of the CSA patterns at slow spinning speeds[47,65]. In our case, moderately fast spinning, only very few labels, weak dipolar interactions (~390 Hz) and the absence of J-couplings should not lead to significant broadening of the CSA pattern as it was verified by SIMPSON simulations (Supplementary Figure S4).

Figure 6 shows the experimental powder patterns of C-3^1 in the acetyl groups of P_L and P_M as well as their simulations which matched the experimental data best. Table 2 shows the experimentally obtained isotropic and anisotropic chemical shift values of P_L and P_M compared to the theoretically obtained isotropic and anisotropic chemical shift values obtained from the DFT calculations where His-L168 is protonated either in τ- or π-position (model A or B). The difference in the principal values of the CSA (δ_{11}-δ_{33}) of the two molecules show an unequal coordination mode of the two acetyl groups suggesting a hydrogen bond between the acetyl group of P_L and His-L168.

The observed experimental anisotropy values δ_{aniso} of both powder patterns (12 kHz $\cong$ 120 ppm (P_L) and 11.3 kHz $\cong$ 112 ppm (P_M)) are larger than the anisotropy values of the carboxylate group in glycine ($\delta_{aniso} \cong$ 7.5 kHz) providing strong evidence for the high rigidity of the system[47]. Motions with a correlation time $\tau_c \ll$ 85 µs would lead to an averaging of the CSA, which is in the time scale of multiple photocycles in RC of *R. sphaeroides* WT[66]. Since the sample is under continuous illumination and therefore passes multiple photocycles during each scan, the size of the anisotropy implies that the acetyl group, if there is any structural change related to this group, does not remain changed on the timescale of nanoseconds or longer. If the acetyl group of P_L would be changing its orientation, the movement in both directions need to be on a ps time scale that is not observable with this experiment.
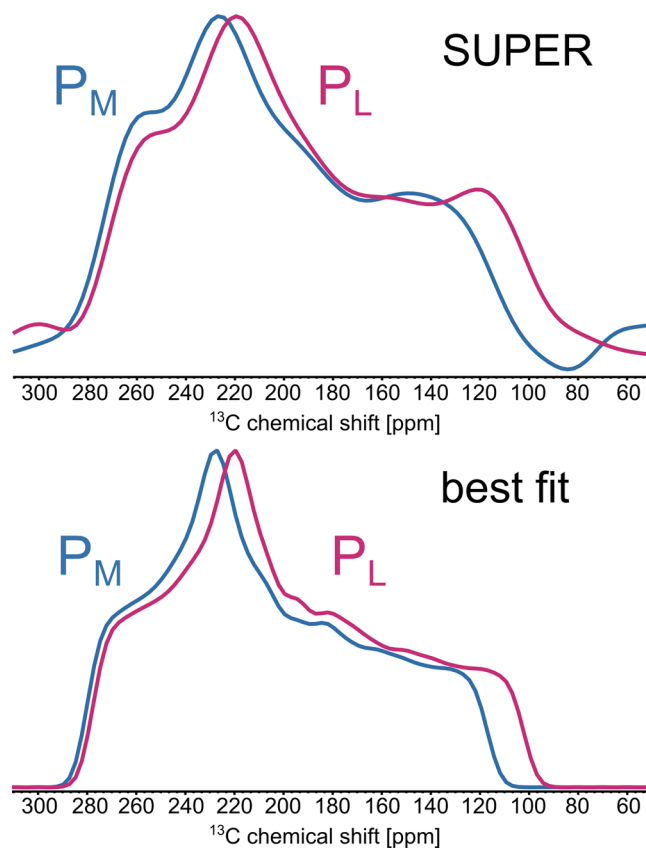
5

Figure 6. Cross section from the experimental 2D SUPER spectra (top) and the best fit (bottom) patterns of the C-3^1-carbon in the acetyl groups of P_M and P_L. The principal values of the best fit are summarized in Tab. 2 in the "Experiment P_L" and "Experiment P_M" column.

	Experiment P_L	DFT P_L	DFT P_L	Experiment P_M	DFT P_M	DFT P_M
Model	—	A	B	—	A	B
δ_{iso} [ppm]	194.1	195.3	204.6	196.3	201.9	200.8
δ_{aniso} [ppm]	-120 ± 2	-107	-120	-112 ± 2	-114	-114
η [−]	0.60 ± 0.04	0.24	0.09	0.58 ± 0.04	0.09	0.16
δ_{11} [ppm]	290	262	270	285	269	267
δ_{22} [ppm]	218	236	259	220	249	249
δ_{33} [ppm]	74	88	85	85	88	87

Table 2. Experimental (best fit from Fig. 2) and calculated isotropic chemical shift δ_{iso}, reduced anisotropy δ_{aniso} and principal values $\delta_{11} - \delta_{33}$ of the CSA tensor according to IUPAC of the acetyl groups of the two special pair molecules P_L and P_M.

The calculated isotropic chemical shifts of C-3^1 of P_L show a reasonable agreement for model A. If His-L168 is protonated in the π-position (model B), the calculated isotropic chemical shift is off by about 10 ppm as C-3^1 of P_L is coordinated to the magnesium ion of P_M. The isotropic chemical shift as well as the principal values of the chemical shift anisotropy of C-3^1 of P_M are independent of the protonation state of His-L168. We note, however, that the calculated values are off by about 5 ppm which is within the expected error of the employed approach[67]. Unfortunately, we are limited to GGA calculations due to the size of the system. Since the principal CSA values are caused by the electronic environment of the observed nucleus, the differences in the principal CSA values might therefore also be caused by differences in geometry of the model compared to the experimental case which is assumed to be close to the crystal structure. In this case, the high accuracy of the NMR data might be used to recalculate the orientation of the acetyl group and therefore for refinement of the arrangement of the cofactor in the protein pocket.

The findings are also in agreement with the observations of Li and Hong stating that the π-tautomer of histidine is only formed as an anionic tautomer at high pH and is metastable in the presence of water suggesting a short lifetime[68]. Hence, a stabilization of the π-tautomer of His-L168 can only be achieved by further metal-ion coordination or H-bonding, which is implausible in this case[68,69]. Therefore, we assume that His-L168 is protonated in the τ-position.

Conclusion

We used the selectivity and the strong enhancement of solid-state photo-CIDNP MAS NMR to identify and probe the dynamics of the two acetyl groups in the Special Pair of *R. sphaeroides* WT by measuring the isotropic chemical shifts and principal values of their CSA tensors. In conjunction with DFT calculations, we showed that a rigid hydrogen bond between His-L168 and the acetyl group of P_L is present. The high values of the reduced anisotropy of the CSA of both acetyl groups imply that they are not changing their orientation on the time scale of ns to µs. This suggests that if the acetyl-group of P_L is flipping to act as a valve preventing fast charge-recombination, the flip has to happen on the ps time scale after the light-induced electron transfer.

References

1. Deisenhofer, J. & Michel, H. In *Molecular Mechanisms in Bioenergetics* (ed. Ernster, L.) 103–120 (Elsevier Science Publishing, 1992).
2. Holzwarth, A. R. & Müller, M. G. Energetics and Kinetics of Radical Pairs in Reaction Centers from Rhodobacter sphaeroides. A Femtosecond Transient Absorption Study. *Biochemistry* **35**, 11820–11831 (1996).
3. Céspedes-Camacho, I. F. & Matysik, J. In *The Biophysics of Photosynthesis* 141–170, https://doi.org/10.1007/978-1-4939-1148-6_5 (Springer New York, 2014).
4. Allen, J. P. *et al*. EPR, ENDOR, and Special TRIPLE measurements of P•+ in wild type and modified reaction centers from Rb. sphaeroides. *Photosynth. Res.* **99**, 1–10 (2009).
5. Lendzian, F. *et al*. The electronic structure of the primary donor cation radical in Rhodobacter sphaeroides R-26: ENDOR and TRIPLE resonance studies in single crystals of reaction centers. *BBA - Bioenerg.* **1183**, 139–160 (1993).
6. Rautter, J., Lendzian, F., Lubitz, W., Wang, S. & Allen, J. P. Comparative Study of Reaction Centers from Photosynthetic Purple Bacteria: Electron Paramagnetic Resonance and Electron Nuclear Double Resonance Spectroscopy. *Biochemistry* **33**, 12077–12084 (1994).
7. Lubitz, W., Lendzian, F. & Bittl, R. Radicals, radical pairs and triplet states in photosynthesis. *Acc. Chem. Res.* **35**, 313–320 (2002).
8. Thamarath, S. S. *et al*. Electron spin density distribution in the special pair triplet of rhodobacter sphaeroides R26 revealed by magnetic field dependence of the solid-state photo-CIDNP effect. *J. Am. Chem. Soc.* **134**, 5921–5930 (2012).
9. Schulten, E. A. M. *et al*. 13C MAS NMR and Photo-CIDNP Reveal a Pronounced Asymmetry in the Electronic Ground State of the Special Pair of Rhodobacter sphaeroides Reaction Centers. *Biochemistry* **41**, 8708–8717 (2002).
10. Prakash, S. *et al*. 13C Chemical Shift Map of the Active Cofactors in Photosynthetic Reaction Centers of Rhodobacter sphaeroides Revealed by Photo-CIDNP MAS NMR. *Biochemistry* **46**, 8953–8960 (2007).
11. Daviso, E. *et al*. The electronic structure of the primary electron donor of reaction centers of purple bacteria at atomic resolution as observed by photo-CIDNP 13 C NMR. *Proc. Natl. Acad. Sci.* **106**, 22281–22286 (2009).
12. Sai Sankar Gupta, K. B., Alia, A., de Groot, H. J. M. & Matysik, J. Symmetry break of special pair: Photochemically induced dynamic nuclear polarization NMR confirms control by nonaromatic substituents. *J. Am. Chem. Soc.* **135**, 10382–10387 (2013).
13. Sai Sankar Gupta, K. B. *et al*. Spectral editing through laser-flash excitation in two-dimensional photo-CIDNP MAS NMR experiments. *J. Magn. Reson.* **246**, 9–17 (2014).
14. Muegge, I. *et al*. Shift of the Special Pair Redox Potential: Electrostatic Energy Computations of Mutants of the Reaction Center from Rhodobacter sphaeroides †. *Biochemistry* **35**, 8359–8370 (1996).
15. Apostolakis, J., Muegge, I., Ermler, U., Fritzsch, G. & Knapp, E. W. Free Energy Computations on the Shift of the Special Pair Redox Potential: Mutants of the Reaction Center of Rhodobacter sphaeroides. *J. Am. Chem. Soc.* **118**, 3743–3752 (1996).
16. Wawrzyniak, P. K., Beerepoot, M. T. P., de Groot, H. J. M. & Buda, F. Acetyl group orientation modulates the electronic ground-state asymmetry of the special pair in purple bacterial reaction centers. *Phys. Chem. Chem. Phys.* **13**, 10270–10279 (2011).
17. Ermler, U., Fritzsch, G., Buchanan, S. K. & Michel, H. Structure of the photosynthetic reaction centre from Rhodobacter sphaeroides at 2.65 å resolution: cofactors and protein-cofactor interactions. *Structure* **2**, 925–936 (1994).
18. Hutter, M. C., Hughes, J. M., Reimers, J. R. & Hush, N. S. Modeling the bacterial photosynthetic reaction center. 2. A combined quantum mechanical molecular mechanical study of the structure of the cofactors in the reaction centers of purple bacteria. *J. Phys. Chem. B* **103**, 4906–4915 (1999).
19. Wadsten, P. *et al*. Lipidic Sponge Phase Crystallization of Membrane Proteins. *J. Mol. Biol.* **364**, 44–53 (2006).
20. Sebban, P. *et al*. pH Modulates the Quinone Position in the Photosynthetic Reaction Center from Rhodobacter sphaeroides in the Neutral and Charge Separated States. *J. Mol. Biol.* **371**, 396–409 (2007).
21. Mattioli, T. A., Williams, J. A. C., Allen, J. P. & Robert, B. Changes in Primary Donor Hydrogen-Bonding Interactions in Mutant Reaction Centers from Rhodobacter sphaeroides: Identification of the Vibrational Frequencies of All the Conjugated Carbonyl Groups. *Biochemistry* **33**, 1636–1643 (1994).
22. Mattioli, T. A., Lin, X., Allen, J. P. & Williams, J. C. Correlation between Multiple Hydrogen Bonding and Alteration of the Oxidation Potential of the Bacteriochlorophyll Dimer of Reaction Centers from Rhodobacter sphaeroides. *Biochemistry* **34**, 6142–6152 (1995).
23. Hughes, J. M., Hutter, M. C., Reimers, J. R. & Hush, N. S. Modeling the Bacterial Photosynthetic Reaction Center. 4. The Structural, Electrochemical, and Hydrogen-Bonding Properties of 22 Mutants of Rhodobacter sphaeroides. *J. Am. Chem. Soc.* **123**, 8550–8563 (2001).
24. Rubin, A. B. *et al*. Polarization effects in photosynthetic membranes. *Int. J. Quantum Chem.* **17**, 587–593 (1980).
25. Trissl, H.-W., Bernhardt, K. & Lapin, M. Evidence for Protein Dielectric Relaxations in Reaction Centers Associated with the Primary Charge Separation Detected from Rhodospirillum rubrum Chromatophores by Combined Photovoltage and Absorption Measurements in the 1−15 ns Time Range †. *Biochemistry* **40**, 5290–5298 (2001).
26. Sham, Y. Y., Muegge, I. & Warshel, A. The Effect of Protein Relaxation on Charge-Charge Interactions and Dielectric Constants of Proteins. *Biophys. J.* **74**, 1744–1753 (1998).
27. Daviso, E., Jeschke, G. & Matysik, J. In *Biophysical Techniques in Photosynthesis. Advances in Photosynthesis and Respiration* (eds Aartsma, T. J. & Matysik, J.) 385–399, https://doi.org/10.1007/978-1-4020-8250-4_19 (Springer, Dordrecht, 2008).
28. Bode, B. E. *et al*. In *Hyperpolarization Methods in NMR Spectroscopy* (ed. Kuhn, L. T.) 1, 105–121 (Springer-Verlag Berlin Heidelberg, 2013).
29. Zysmilich, M. G. & McDermott, A. E. Photochemically Induced Dynamic Nuclear Polarization in the Solid-State 15N Spectra of Reaction Centers from Photosynthetic Bacteria Rhodobacter sphaeroides R-26. *J. Am. Chem. Soc.* **116**, 8362–8363 (1994).
30. Zysmilich, M. G. & McDermott, A. E. Natural abundance solid-state carbon NMR studies of photosynthetic reaction centers with photoinduced polarization. *Proc Natl Acad Sci USA* **93**, 6857–6860 (1996).
31. Matysik, J. *et al*. A set-up to study photochemically induced dynamic nuclear polarization in photosynthetic reaction centres by solid-state NMR. *Indian J. Biochem. Biophys.* **37**, 418–23 (2000).
32. Alia *et al*. Photochemically induced dynamic nuclear polarization in photosystem I of plants observed by 13C magic-angle spinning NMR. *J. Am. Chem. Soc.* **126**, 12819–12826 (2004).
33. Thamarath, S. S., Heberle, J., Hore, P. J., Kottke, T. & Matysik, J. Solid-state photo-CIDNP effect observed in phototropin LOV1-C57S by 13C magic-angle spinning NMR spectroscopy. *J. Am. Chem. Soc.* **132**, 15542–15543 (2010).
34. Zill, J. C. *et al*. Photo-CIDNP in the Reaction Center of the Diatom Cyclotella meneghiniana Observed by13C MAS NMR the solid-state photo-CIDNP effect in a new kingdom of the tree of life. *Zeitschrift fur Phys. Chemie* **231**, 347–367 (2017).

35. Zill, J. C. *et al*. 15N photo-CIDNP MAS NMR on both photosystems and magnetic field-dependent13C photo-CIDNP MAS NMR in photosystem II of the diatom Phaeodactylum tricornutum. *Photosynth. Res*. 1–21, https://doi.org/10.1007/s11120-018-0578-9 (2018).
36. Zill, J. C. *et al*. 15N photo-CIDNP MAS NMR analysis of reaction centers of Chloracidobacterium thermophilum. *Photosynth. Res*. **137**, 295–305 (2018).
37. Janssen, G. J. *et al*. Photochemically induced dynamic nuclear polarization NMR on photosystem II: donor cofactor observed in entire plant. *Sci. Rep.* **8**, 17853 (2018).
38. Jeschke, G. A new mechanism for chemically induced dynamic nuclear polarization in the solid state. *J. Am. Chem. Soc.* **120**, 4425–4429 (1998).
39. Polenova, T. & McDermott, A. E. A Coherent Mixing Mechanism Explains the Photoinduced Nuclear Polarization in Photosynthetic Reaction Centers. *J. Phys. Chem. B* **103**, 535–548 (1999).
40. Jeschke, G. & Matysik, J. A reassessment of the origin of photochemically induced dynamic nuclear polarization effects in solids. *Chem. Phys.* **294**, 239–255 (2003).
41. Sosnovsky, D. V., Jeschke, G., Matysik, J., Vieth, H. M. & Ivanov, K. L. Level crossing analysis of chemically induced dynamic nuclear polarization: Towards a common description of liquid-state and solid-state cases. *J. Chem. Phys.* **144**, 144202 (2016).
42. Sosnovsky, D. V. *et al*. Magnetic field and orientation dependence of solid-state CIDNP. *J. Chem. Phys.* https://doi.org/10.1063/1.5077078 (2019).
43. Fischer, M. R. *et al*. Carbon-13 magic angle spinning NMR study of the light-induced and temperature-dependent changes in Rhodobacter sphaeroides R26 reaction centers enriched in [4′-13C]tyrosine. *Biochemistry* **31**, 11038–11049 (1992).
44. Thakur, R. S., Kurur, N. D. & Madhu, P. K. Swept-frequency two-pulse phase modulation for heteronuclear dipolar decoupling in solid-state NMR. *Chem. Phys. Lett.* **426**, 459–463 (2006).
45. Kristiansen, P. E., Carravetta, M., Lai, W. C. & Levitt, M. H. A robust pulse sequence for the determination of small homonuclear dipolar couplings in magic-angle spinning NMR. *Chem. Phys. Lett.* **390**, 1–7 (2004).
46. Märker, K., Hediger, S. & De Paëpe, G. Efficient 2D double-quantum solid-state NMR spectroscopy with large spectral widths. *Chem. Commun.* **53**, 9155–9158 (2017).
47. Liu, S.-F., Mao, J.-D. & Schmidt-Rohr, K. A Robust Technique for Two-Dimensional Separation of Undistorted Chemical-Shift Anisotropy Powder Patterns in Magic-Angle-Spinning NMR. *J. Magn. Reson.* **155**, 15–28 (2002).
48. Marion, D., Ikura, M., Tschudin, R. & Bax, A. Rapid recording of 2D NMR spectra without phase cycling. Application to the study of hydrogen exchange in proteins. *J. Magn. Reson.* **85**, 393–399 (1989).
49. Bak, M., Rasmussen, J. T. & Nielsen, N. C. SIMPSON: A General Simulation Program for Solid-State NMR Spectroscopy. *J. Magn. Reson.* 147, (296–330 (2000).
50. Camara-Artigas, A., Brune, D. & Allen, J. P. Interactions between lipids and bacterial reaction centers determined by protein crystallography. *Proc. Natl. Acad. Sci.* **99**, 11055–11060 (2002).
51. Neese, F. The ORCA program system. Wiley Interdiscip. Rev. *Comput. Mol. Sci.* **2**, 73–78 (2012).
52. Lee, C., Yang, W. & Parr, R. G. Development of the Colle-Salvetti correlation-energy formula into a functional of the electron density. *Phys. Rev. B* **37**, 785–789 (1988).
53. Weigend, F. & Ahlrichs, R. Balanced basis sets of split valence, triple zeta valence and quadruple zeta valence quality for H to Rn: Design and assessment of accuracy. *Phys. Chem. Chem. Phys.* **7**, 3297 (2005).
54. Weigend, F. Accurate Coulomb-fitting basis sets for H to Rn. *Phys. Chem. Chem. Phys.* **8**, 1057 (2006).
55. Grimme, S., Antony, J., Ehrlich, S. & Krieg, H. A consistent and accurate ab initio parametrization of density functional dispersion correction (DFT-D) for the 94 elements H-Pu. *J. Chem. Phys.* **132**, 154104 (2010).
56. Grimme, S., Ehrlich, S. & Goerigk, L. Effect of the damping function in dispersion corrected density functional theory. *J. Comput. Chem.* **32**, 1456–1465 (2011).
57. Takano, Y. & Houk, K. N. Benchmarking the Conductor-like Polarizable Continuum Model (CPCM) for Aqueous Solvation Free Energies of Neutral and Ionic Organic Molecules. *J. Chem. Theory Comput.* **1**, 70–77 (2005).
58. Daviso, E. *et al*. Electron−Nuclear Spin Dynamics in a Bacterial Photosynthetic Reaction Center. *J. Phys. Chem. C* **113**, 10269–10278 (2009).
59. Roy, E. *et al*. Characterization of the Primary Radical Pair in Reaction Centers of Heliobacillus mobilis by 13C Photo-CIDNP MAS NMR. *Biochemistry* **47**, 4629–4635 (2008).
60. Janssen, G. J. *et al*. Observation of the solid-state photo-CIDNP effect in entire cells of cyanobacteria Synechocystis. *Photosynth. Res.* **104**, 275–282 (2010).
61. Thamarath, S. S. *et al*. Whole Cell Nuclear Magnetic Resonance Characterization of Two Photochemically Active States of the Photosynthetic Reaction Center in Heliobacteria. *Biochemistry* **51**, 5763–5773 (2012).
62. Najdanova, M., Gräsing, D., Alia, A. & Matysik, J. Analysis of the Electronic Structure of the Special Pair of a Bacterial Photosynthetic Reaction Center by 13C Photochemically Induced Dynamic Nuclear Polarization Magic-Angle Spinning NMR Using a Double-Quantum Axis. *Photochem. Photobiol.* **94**, 69–80 (2018).
63. Prakash, S. *et al*. Magnetic field dependence of photo-CIDNP MAS NMR on photosynthetic reaction centers of Rhodobacter sphaeroides WT. *J. Am. Chem. Soc.* **127**, 14290–14298 (2005).
64. Gräsing, D. *et al*. Field-cycling NMR with high-resolution detection under magic-angle spinning: determination of field-window for nuclear hyperpolarization in a photosynthetic reaction center. *Sci. Rep.* **7**, 12111 (2017).
65. Hong, M. & Yao, X. Homonuclear decoupled chemical shift anisotropy in doubly labeled peptides by selective-pulse solid-state NMR. *J. Magn. Reson.* **160**, 114–119 (2003).
66. Hoff, A. J. & Deisenhofer, J. Photophysics of photosynthesis. *Structure and spectroscopy of reaction centers of purple bacteria. Phys. Rep.* **287**, 1–247 (1997).
67. Reiter, K., Mack, F. & Weigend, F. Calculation of Magnetic Shielding Constants with meta-GGA Functionals Employing the Multipole-Accelerated Resolution of the Identity: Implementation and Assessment of Accuracy and Efficiency. *J. Chem. Theory Comput.* **14**, 191–197 (2018).
68. Li, S. & Hong, M. Protonation, tautomerization, and rotameric structure of histidine: A comprehensive study by magic-angle-spinning solid-state NMR. *J. Am. Chem. Soc.* **133**, 1534–1544 (2011).
69. Haddad, K. C., Sudmeier, J. L., Bachovchin, D. A. & Bachovchin, W. W. alpha-Lytic protease can exist in two separately stable conformations with different His57 mobilities and catalytic activities. *Proc. Natl. Acad. Sci.* **102**, 1006–1011 (2005).

Acknowledgements

Author Contributions

Daniel Gräsing: performed experiments, wrote the paper. Katarzyna M. Dziubińska-Kühn: performed the DFT calculations. Stefan Zahn: designed the research, performed the DFT calculations, wrote the paper. A. Alia: prepared the sample, wrote the paper. Jörg Matysik: designed the research, wrote the paper.

Additional Information

Supplementary information accompanies this paper at https://doi.org/10.1038/s41598-019-46903-4.

Competing Interests: The authors declare no competing interests.

Publisher's note: Springer Nature remains neutral with regard to jurisdictional claims in published maps and institutional affiliations.